Numerical modeling of the behavior of an elastic capsule in a microchannel flow: The initial motion

Gang Ma,[1] Jinsong Hua,[2] and Hua Li[1,*]

[1]*School of Mechanical and Aerospace Engineering, Nanyang Technological University, Singapore 639798, Singapore*

[2]*Department of Process and Fluid Flow Technology, Institute for Energy Technology, P.O. Box 40, N-2027 Kjeller, Norway*

(Received 3 October 2008; published 21 April 2009)

The initial motion of two-dimensional capsule in microchannel flow just after release is investigated in this paper by a numerical simulation method, which combines the finite volume method with the front tracking technique. The capsule is modeled as liquid medium enclosed by a thin membrane, for which linear elastic properties are taken into consideration. Three kinds of initial capsule shapes (circle, ellipse, and biconcave) and three initial positions (center-line, near-center, and near-wall positions) are considered in the simulations. Off-center capsules (the near-center and near-wall capsules) experience tilting and membrane tank-treading, and migrate laterally while they move with the fluid flow. After initial rapid tilting, the circular and elliptic near-wall capsules reach quasistationary tilt orientation, while the biconcave near-wall capsules experience steady change in tilt orientation with time. Lateral movements of the capsules indicate the existence of lift effect causing the capsule to move away from the wall. Lift velocities, the velocity components along the transverse direction, of the circular near-wall capsules decrease as they approach the centerline, while those of the elliptic and biconcave near-wall capsules do not show this trend, which might result from the short range of the simulation time. In general, the capsule with higher membrane dilation modulus has lower lift velocity, showing the effect of capsule deformability on the capsule behavior. Both tank-treading and lift velocities are 1–2 orders lower than the capsule translational velocity. For the circular and biconcave capsules, no matter the center-line or off-center capsules, hematocrit ratio increases with the membrane dilation modulus, namely, the capsule moving velocity decreases with the increasing dilation modulus, while the elliptic capsules with nondimensional membrane dilation moduli of 2500 and 500 show inverse trend in some time range. A preliminary study is carried out for long-term simulation of a circular capsule.

DOI: 10.1103/PhysRevE.79.046710 PACS number(s): 47.11.−j, 87.16.A−, 83.50.Ha, 87.16.D−

I. INTRODUCTION

The mechanics of red blood cells flowing in blood vessels or small tubes has been studied experimentally [1], theoretically [2], or numerically [3] because of its importance in physiology. Vesicles have also been investigated [4] because they are extensively used in cosmetic, pharmaceutical or agricultural industries, and they also can be used as model systems for studying the properties of red blood cells. Red blood cell and vesicle are examples of capsules that consist of a liquid internal medium enclosed by a thin deformable membrane. In normal state, human red blood cells are in biconcave shape with a maximum diameter of about 8 μm and a thickness of about 2 μm. When blood cells flow in small tube, they may experience high stress and large deformation. The mechanical behaviors, for example, the deformability, of single red blood cells through microcapillaries are relevant to the rheological properties of blood in microcirculation and even to the overall hydrodynamics of large-scale blood flow [5]. Hence, it is of great importance to develop a suitable physical model to analyze the cell/vesicle behavior with channel flow, and understanding the dynamics of individual capsule under different conditions is the first step in studying the rheological properties of capsule suspension. A number of theoretical and numerical studies have been conducted with focus on the behavior of cell/vesicle in small sized tube or constriction to predict their deformation and to estimate the effective or apparent viscosity of cell/vesicle suspension.

When analyzing problem of tightly fitting particles, where a thin film of liquid exists between the particle and the capillary wall, a lubrication method can be used to model the flow in the narrow gaps. The motions of red blood cells in narrow tubes were studied by Secomb [6] and Halpern and Secomb [7] by using the lubrication method. Under certain conditions, the cell shapes were predicted to be round and convex in the front and concave at the rear in flow [6], agreeing with experimental observations. Secomb and Hsu [2] adopted a time-dependent lubrication method to study the motion of red cells with surface area conservation through cylindrical micropores. All the studies above mentioned were about the axisymmetric motion of red cells through capillaries or micropores. Generally, the cells assume nonaxisymmetric configurations in flows. Secomb and Skalak [8] used the lubrication method to study the asymmetric behaviors of cells in two-dimensional (2D) capillary flow and found that the asymmetric cell shapes lead to tank-treading motion of membrane, which reduces the required driving pressure to sustain a given cell velocity. Unfortunately, the lubrication method requires specific shapes [8] and sometimes steady configurations [2], which limits its application in the analysis of motion of deformable capsules in a flow.

Boundary integral method for Stokes flow is one of the popular methods for analyzing capsule behaviors in flow. Its advantage is to relate the velocity of any point within the fluid, including points on the capsule, to the velocity and

*Corresponding author; lihua@ntu.edu.sg

stresses on the boundary, instead of solving the Stokes equations throughout the whole computational domain. It was used by Leyrat-Maurin and Barthes-Biesel [9] and by Queguiner and Barthes-Biesel [10] to study the motion of an initially spherical capsule through constrictions, and by Lefebvre and Barthes-Biesel [11] to study the flow of an initially spherical capsule in a coaxial cylindrical tube, in which isotropic membrane prestress was taken into consideration. Pozrikidis [3] used a boundary integral model to study the motion of a file of red blood cells in capillaries. All these studies were conducted for problems with axisymmetric configurations. As to the asymmetric problem, Kaoui *et al.* [12] used a boundary integral model to study the lateral migration of suspended vesicle in an unbounded two-dimensional Poiseuille flow. The unbounded flow conditions are only approximately satisfied when the capsule size is much smaller than the tube diameter. It is thus required to investigate the capsule behaviors in bounded flow when the tube size is at the same order as the capsule size.

In order to study the motion of capsule in microscale tube, the position and motion of the membrane need to be tracked. So far several techniques have been proposed to track arbitrarily shaped interfaces. They may be classified into the volume tracking and front tracking methods. In the volume tracking methods, marker particles are used to construct the interface [13], or a marker function is used, and advected by the flow [14]. The improvement in the volume tracking methods includes the use of the simple line interface calculation [15]. In order to achieve higher computational accuracy in capsule motion simulation, it is better to employ the front tracking methods, in which the interface itself is represented by a set of additional points [16], while the fluid problem is solved on stationary grid. Early versions of the front tracking methods were used for simulations of particle motion [17] and bubble motion [18] in fluid.

The numerical method used in this paper combines the finite volume technique for solving the fluid problem with the front tracking technique proposed by Unverdi and Tryggvason [18] for capturing and tracking the capsule membrane. It is similar to the method used in [19], in which bubble rising was simulated. The simulation results on bubble rising [19] demonstrate that the algorithm used in the present study is robust in flow regimes with large range of Reynolds number, and density and viscosity ratios. The main difficulties in simulating the motion of capsule in micro flow are how to determine the interactions between membrane and fluid and how to track the capsule membrane. In the present method, a stationary, fixed Eulerian grid is used for the fluid flow, and a set of Lagrangian nodes is used to discretize and represent the membrane. Differences of properties, such as density and viscosity, of fluids inside and outside the membrane are considered, and their values are calculated according to the membrane position based on an indicator function, and the abrupt value jumps are smoothed by using a distribution function instead of δ (Dirac-delta) function [18]. The interactions between capsule membrane and fluid will be deduced based on membrane mechanics. The distribution function is also used to smooth and distribute the concentrated forces on membrane nodes obtained from the membrane mechanics to the neighboring Eulerian grid points. One set of Navier-Stokes equations is solved in the whole computational domain by treating the different phases as one fluid with variable material properties. The membrane position is advected explicitly using the velocity interpolated from the velocity of fluid on the Eulerian grid. By using the distribution function in stead of δ function and calculating the membrane velocity interpolated from background fluid, this method could avoid numerical diffusion, and capture the sharp membrane.

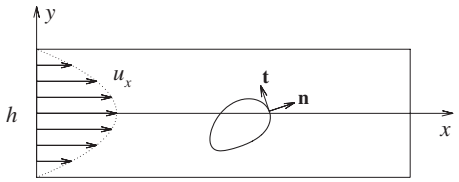

FIG. 1. Schematic illustration of a 2D capsule moving in a microchannel.

Pozrikidis [3] studied the dependence of red blood cell behavior on the nondimensional variable, $G=\mu U_m/E_s$, where μ is the viscosity of suspending liquid, U_m the mean velocity of axisymmetric Poiseuille flow, and E_s the membrane shear modulus, and interpreted the results as affected by the mean velocity. If μ and U_m are kept constant, the effects of membrane mechanical properties on capsule behavior can be elucidated. In literature, different initial particle shapes [3,11] and different initial particle positions [12] have been considered in calculations, and we believe these are important factors influencing the capsule behaviors. The present work is done by short-term simulations for analysis of the initial motion of a 2D capsule in capillary after release, and the effects of elastic dilation modulus of membrane, initial capsule shape, and initial capsule position will be taken into consideration. Capsule membrane obeys linear elastic rules.

This paper is organized as follows. Details of the governing equations, the nondimensionalization of equations, the treatment of discontinuities across the capsule membrane, and the simulation conditions are described in Sec. II. The numerical results corresponding to different membrane dilation moduli, initial capsule shapes, and initial capsule positions are presented and discussed with comparison with other available data in Sec. III. Finally, conclusions drawn from this study are summarized in Sec. IV.

II. MATHEMATICAL FORMULATION

A. Model

In the present paper, the motion of single 2D capsule in flow within 2D capillary tube is studied. The schematic illustration of 2D capsule moving in microchannel is shown in Fig. 1, in which h is the height of the capillary tube, and (x,y) are the coordinates. Surrounding liquid flows from left to right, along the positive x direction. Velocity field of the 2D Poiseuille flow, u_x, is defined as the initial flow velocity field in the whole computational domain, and its y component is zero, as shown in Fig. 1. A 2D capsule is represented by a closed curve, with **t** being the unit tangent vector point-

ing in the anticlockwise direction of increasing arc length l, and $\mathbf{n}$ the unit normal vector. In the presence of capsule, material properties of fluid phases inside and outside the capsule membrane may be different. Here, one set of governing equations, Navier-Stokes equations, is solved in the whole computational domain by treating the different phases as one fluid with variable material properties. The Navier-Stokes equations are given as

$$\frac{\partial(\rho\mathbf{u})}{\partial t} + \nabla \cdot \rho\mathbf{u}\mathbf{u} = -\nabla p + \nabla \cdot [\mu(\nabla\mathbf{u} + \nabla^{\mathrm{T}}\mathbf{u})] + \mathbf{F}, \quad (1)$$

where ρ and μ are the density and viscosity of fluid, respectively, p the pressure in fluid, $\mathbf{u}$ the fluid velocity vector, t time, and $\mathbf{F}$ the body force acted on fluid by capsule membrane.

The body force $\mathbf{F}$ in Eq. (1), which reflects the interaction between the capsule membrane and fluid, can be deduced by the equilibrium of membrane. The vectorial tension exerted on a 2D membrane is given by

$$\mathbf{T} = \tau\mathbf{t} + q\mathbf{n}, \quad (2)$$

where τ is the in-plane tension, and q is the transverse tension. The membrane load, which is the discontinuity in the surface traction across the membrane, can be obtained through a force balance over an infinitesimal section of the membrane [20], and given by

$$\Delta\mathbf{f} = \Delta f^n\mathbf{n} + \Delta f^t\mathbf{t} = -\frac{d\mathbf{T}}{dl} = -\frac{d}{dl}(\tau\mathbf{t} + q\mathbf{n}). \quad (3)$$

Using the relations, $\frac{d\mathbf{t}}{dl} = -\kappa\mathbf{n}$ and $\frac{d\mathbf{n}}{dl} = \kappa\mathbf{t}$, where κ is the curvature of the membrane, and the expression for the transverse shear tension in terms of the bending moment $q = \frac{dm}{dl}$, one has the following normal and tangential membrane loads

$$\Delta f^n = \kappa\tau - \frac{d^2m}{dl^2}, \quad \Delta f^t = -\frac{d\tau}{dl} - \kappa\frac{dm}{dl}. \quad (4)$$

Let E_M and E_B be the area elastic dilation modulus and bending stiffness, respectively, the in-plane tension is expressed as $\tau = E_M\varepsilon$, where ε is the tensile strain of membrane, and the bending moment is $m = E_B\Delta\kappa = E_B(\kappa - \kappa_0)$, where κ_0 is the membrane resting curvature. The equilibrium equations can thus be expressed as

$$\Delta f^n = E_M\kappa\varepsilon - E_B\frac{d^2\kappa}{dl^2}, \quad \Delta f^t = -E_M\frac{d\varepsilon}{dl} - E_B\kappa\frac{d\kappa}{dl}. \quad (5)$$

In simulations, the regular Eulerian grid is used to discretize the 2D computational domain of fluid, while the capsule membrane is discretized by a group of Lagrangian nodes. The straight segments connecting successive Lagrangian nodes are the membrane elements. The fluid force, $\mathbf{F}_{\mathrm{node}}$, which is defined on the membrane nodes, can be calculated by integrating the membrane load characterized by Eq. (5). Then the concentrated force acted on fluid by the membrane is

$$\mathbf{F}_{\mathrm{fluid}} = -\mathbf{F}_{\mathrm{node}}, \quad (6)$$

which is also defined on the membrane nodes. In order to solve the governing Eq. (1), it is required to compute the force acted on the fluid and defined on the fluid grid points based on the knowledge of $\mathbf{F}_{\mathrm{fluid}}$. This will be discussed further in the following section.

Several nondimensional variables are introduced as follows:

$$x^* = \frac{x}{x_0}, \quad u^* = \frac{u}{u_l}, \quad \rho^* = \frac{\rho}{\rho_l},$$

$$\mu^* = \frac{\mu}{\mu_l}, \quad t^* = \frac{t}{x_0/u_l}, \quad p^* = \frac{p}{\rho_l u_l^2}, \quad (7)$$

where x_0, u_l, ρ_l, μ_l, x_0/u_l, and $\rho_l u_l^2$ are the characteristic variables for nondimensionalization. The nondimensionalized Navier-Stokes equation is obtained as

$$\frac{\partial(\rho\mathbf{u})}{\partial t} + \nabla \cdot \rho\mathbf{u}\mathbf{u} = -\nabla p + \frac{1}{\mathrm{Re}}\nabla \cdot [\mu(\nabla\mathbf{u} + \nabla^{\mathrm{T}}\mathbf{u})] + \mathbf{F} \quad (8)$$

in which the superscript * is omitted for convenience. The nondimensional Reynolds number is defined as follows:

$$R_e = \frac{\rho_l u_l x_0}{\mu_l}. \quad (9)$$

According to the nondimensionalization approach, the area dilation modulus and bending stiffness of membrane are nondimensionalized as

$$E_m = E_M/(\rho_l u_l^2 x_0), \quad E_b = E_B/(\rho_l u_l^2 x_0^3). \quad (10)$$

B. Treatment of the discontinuities across the membrane

The fluids inside and outside capsule membrane are unnecessarily the same, so that the properties, density and viscosity, in these two domains may be different, and then abrupt value jumps exist across the membrane. To treat these discontinuities, the field distributions $b(\mathbf{x},t)$ of material properties over the whole solution domain are reconstructed by an indicator function $I(\mathbf{x},t)$ [18], which has the value of unity in the first fluid phase (inside the membrane) and zero in the second phase (outside the membrane) at given time t,

$$b(\mathbf{x},t) = b_2 + (b_1 - b_2) \cdot I(\mathbf{x},t) \quad (11)$$

in which b stands for either fluid density or viscosity. The indicator function can be written in form of an integral over the capsule domain $\Omega(t)$ with the interface $\Gamma(t)$, where in fact is the position of the capsule membrane

$$I(\mathbf{x},t) = \int_{\Omega(t)} \delta(\mathbf{x} - \mathbf{x}')d\mathbf{x}', \quad (12)$$

where $\delta(\mathbf{x}-\mathbf{x}')$ is the delta function that has a value of infinite when $\mathbf{x}' = \mathbf{x}$ and zero elsewhere, and its integration (12) is unity when $\mathbf{x}$ is contained in $\Omega(t)$ and zero otherwise. Taking the gradient of the indicator function and transforming the volume integral into an integral over interface yields

$$\nabla I = \int_{\Gamma(t)} \mathbf{n}\delta(\mathbf{x}-\mathbf{x}')ds. \tag{13}$$

Let $\mathbf{G}(\mathbf{x},t)$ be the gradient of the indicator function. Taking the divergence of Eq. (13) leads to

$$\nabla^2 I = \nabla \cdot \int_{\Gamma(t)} \mathbf{n}\delta(\mathbf{x}-\mathbf{x}')ds = \nabla \cdot \mathbf{G}. \tag{14}$$

By solving the above Poisson equation, in which the right-hand side is a function of the known membrane shape and position at time t, the indicator function $I(\mathbf{x},t)$ can be reconstructed. After the indicator function is obtained, the distribution of fluid property can be calculated by Eq. (11).

Unverdi and Tryggvason [18] proposed a front tracking method, in which the membrane is considered to have a finite thickness with the same order as the fluid mesh size, instead of zero thickness. In the transition zone near the membrane, the fluid properties change smoothly and continuously from one side of the interface to the other side. The artificial thickness of the membrane depends on the grid size and is maintained constant during the computation. Hence, this method does not have numerical diffusion across the interface. This can be realized by using a distribution function $D(\mathbf{x})$ to approximate the delta function. This distribution function gives the fraction of the quantity distributed to nearby grid points across the artificial thickness of the membrane. The use of $D(\mathbf{x})$ leads to the following discretized form of the gradient function $\mathbf{G}(\mathbf{x},t)$:

$$\mathbf{G}(\mathbf{x},t) = \sum_f D(\mathbf{x}-\mathbf{x}_f)\mathbf{n}_f \Delta s_f, \tag{15}$$

where $\mathbf{n}_f$ is the unit normal vector at a membrane element with an area of Δs_f whose centroid is $\mathbf{x}_f$. Thus, the sharp jump of the indicator function across the membrane is spread among the nearby grid points. In the present study, the following distribution function [21] is used for the 2D grid system

$$D(\mathbf{x}-\mathbf{x}_f) = D_1(x-x_f)D_2(y-y_f), \tag{16}$$

where the distribution function $D_1(x)$ is given as follows:

$$D_1(x) = \begin{cases} \dfrac{1}{4h_g}\left(1+\cos\dfrac{\pi x}{2h_g}\right) & \text{for } |x| \le 2h_g \\ 0 & \text{elsewhere,} \end{cases} \tag{17}$$

where h_g is the grid size. Function $D_2(y)$ is similar to Eq. (17) with y instead of x.

The body forces $\mathbf{F}$ in Eq. (1) that are acted on fluid and defined on fluid grid can be calculated by using the distribution function (16) to distribute the concentrated forces defined on membrane nodes by Eq. (6) to nearby fluid grid points through

$$\mathbf{F}(\mathbf{x},t) = \sum_f D(\mathbf{x}-\mathbf{x}_f)\mathbf{F}_{\text{fluid}}. \tag{18}$$

During simulation, the membrane position is advected by the membrane velocities interpolated from the fluid velocities on the background grid, and this interpolation is also conducted by using the distribution function (16).

C. Simulation conditions

The motion in microscale flow of 2D capsule with different membrane dilation moduli, initial shapes, and initial positions is simulated in the present study. The nondimensional y coordinate of the computational domain ranges from -1.2 to 1.2, i.e., the height of the capillary tube is 2.4. The nondimensional tube length is 10. The direction of the background flow is from left to right. In the absence of capsule, the background fluid velocity field is given by the 2D Poiseuille profile

$$u_x = 1.5U_m[1-y^2/(0.5h)^2], \quad u_y = 0, \tag{19}$$

where U_m is the mean velocity, equal to two thirds the centerline velocity. At the beginning of simulation, a capsule with zero speed is put in the flow; just like that the capsule appears all at once in the unperturbed background velocity field. Three kinds of shapes, namely, circle, ellipse, and biconcave, are used as initial capsule shapes, and they are also used as the corresponding resting shapes. For the elliptic capsule, the ratio of the short axis to the long axis is 0.3. The contour in an azimuthal plane of the biconcave capsule, whose center is at the origin of the coordinate system, can be described in parametric form by the equations [22]

$$x = 0.5a\alpha(0.207 + 2.003\sin^2\phi - 1.123\sin^4\phi)\cos\phi,$$
$$y = a\alpha\sin\phi, \tag{20}$$

where the parameter ϕ varies in the range $0 \le \phi \le 2\pi$. The dimensionless coefficient $\alpha = 1.3858189$ is the ratio of the maximum radius of the biconcave disk to the equivalent cell radius a, which is defined by the equation $V_c = 4\pi a^3/3$, where V_c is the capsule volume. As initial conditions, the long axes of both elliptic and biconcave capsules are placed along y direction, and the short axes along x direction. Three different values of nondimensional membrane dilation modulus, 10 000, 2500, and 500, are used in simulations.

In the present study, the maximum diameter of capsule is defined as the characteristic length (x_0), the mean unperturbed fluid velocity (U_m) as the characteristic velocity, the density of the surrounding liquid as the characteristic density, and the viscosity of the surrounding liquid as the characteristic viscosity. Throughout this paper, unless otherwise mentioned, length is expressed in unit of x_0, time in unit of x_0/U_m, velocity in unit of U_m, and membrane dilation modulus in unit of $\rho_l U_m^2 x_0$. Simulations are conducted at the Reynolds number of 0.01, and at the density ratio and the viscosity ratio of internal fluid to external fluid of 1.098 [23] and 1.0, respectively. The ratio of the reduced bending stiffness to the reduced dilation modulus, $E_b/E_m = 1\times10^{-5}$. As such, the simulation results depend on the membrane dilation modulus, E_m, together with the size of the calculation domain, and the initial shape, the initial position, and the resting shape of capsule. For given ρ_l, x_0, and u_l, the effect of membrane elastic property on the capsule behavior can be analyzed. If ρ_l, x_0, and E_M are specified, and Re number (9)

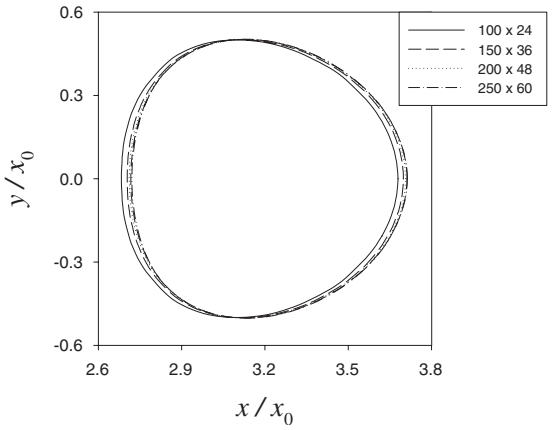

FIG. 2. Effect of grid size on the shapes of circular capsules at nondimensional time 1.6.

is constant, the effect of the mean velocity or the viscosity of the surrounding liquid on the capsule behavior can be elucidated, similar to the study in [3].

In the present simulations, the capsule morphological properties are also determined, which are calculated based on the zero-, first-, and second-order moments of capsule shape, as proposed by Dunn and Brown [24]. Three morphological measures (extension, dispersion, and orientation) are calculated in the present study, and the details of the formulations are provided in the Appendix. Extension, m_{ext}, is a dimensionless measure of how much the shape differs from a circle. When the shape is circular, it equals to zero. It increases without limit as the shape becomes less compact. Dispersion, m_{dis}, another dimensionless measure, quantifies the difference between the shape of a 2D object and its equimomental ellipse. Dispersion of an ellipse is zero, and it increases with the irregularity of the object. Orientation, m_{or}, is the angle of the long axis of the equimomental ellipse with respect to the positive x direction. The calculations of extension and dispersion take into consideration the information of the whole capsule shape, such that they are more suitable for describing the geometrical properties of a 2D shape than the Taylor deformation parameter, which is related only to the length and width of the 2D shape. Also provided in the Appendix is the calculation of the shape centroid position, based on which the capsule center velocity can be determined.

Several numerical tests are conducted for choosing suitable values of simulation parameters. Sensitivity analysis of the background fluid grid is first performed. Here the circular capsule is used in calculations, where the membrane dilation modulus is 2500, and the initial capsule center position is (1.0, 0.0). Capsule membrane is discretized by 160 nodes. The grid sizes are 100×24, 150×36, 200×48, and 250×60, corresponding to 10, 15, 20, and 25 grids, respectively, in unit length. Positions and shapes of capsules at time 1.6 corresponding to different grid sizes are shown in Fig. 2. The figure demonstrates that no significant differences exist in the simulation results for grid sizes of 150×36, 200×48, and 250×60. Taking precision and time consumption into consideration, the grid size of 200×48 is chosen as the basis for the following simulations. The maximum diameter of capsule is then meshed with about 20 grids. Effect of number of nodes discretizing the capsule membrane is also studied. Circular capsule with the same membrane dilation modulus and initial center position as in background grid sensitivity analysis is used here. Grid size of 200×48 is adopted according to the previous numerical test. In this group of simulations, the capsule membrane is discretized by 80, 120, 160, 200, and 240 nodes, respectively. Positions and shapes of capsules at time 3.0 are shown in Fig. 3(a), in which the capsules corresponding to 120, 160, 200, and 240 discretizing nodes coincide. In order to demonstrate the effect of number of membrane nodes clearly, the evolutions of capsule extension are shown in Fig. 3(b). Based on the results in Fig. 3(b), the capsule membrane will be discretized by 200 nodes in the following simulations. The initial position is one of the factors influencing the capsule behavior and the effects of its y component on the capsule motion will be discussed in Sec. III. In the simulations, the capsule starts from the position near to the left boundary of the computational domain, which might affect the capsule motion. Simulations are conducted for the capsules with different initial x positions in order to choose the suitable x coordinate of the initial capsule center position. Circular capsule with membrane dilation modulus of 2500 is adopted in the simulations, where the capsule

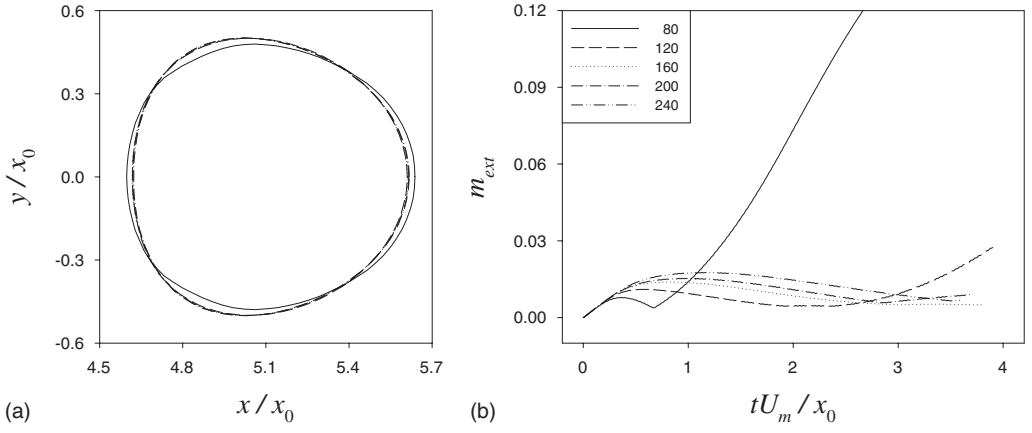

FIG. 3. Effect of number of nodes discretizing the capsule membrane on the shapes of circular capsules at nondimensional time 3.0 (a), and on the extension of 2D capsule shapes (b).

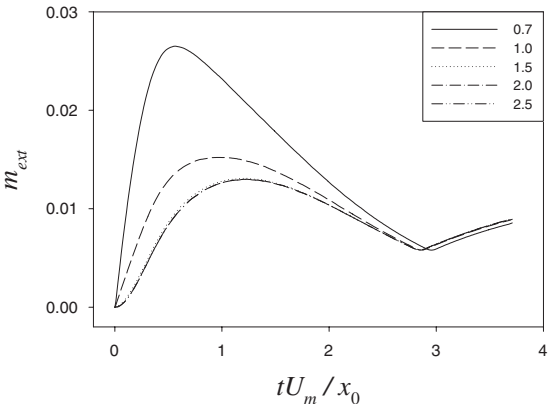

FIG. 4. Effect of nondimensional x coordinate of initial capsule center on the extension of capsules.

membrane is discretized by 200 nodes. Five initial center positions, (0.7, 0.0), (1.0, 0.0), (1.5, 0.0), (2.0, 0.0), and (2.5, 0.0), are considered in calculations, and the evolutions of capsule extension are illustrate in Fig. 4. Difference between results based on the initial x coordinates of 2.0 and 2.5 cannot be distinguished. 2.0 is chosen as the initial x coordinate of capsule center in the following simulations.

In order to simulate the motion of 2D capsule moving with flow, three kinds of initial capsule center positions are considered. The first kind of initial position is (2.0, 0), meaning that capsule stays on the symmetric axis of the background fluid velocity field, and the corresponding case is termed the center-line case. For the second kind, termed the near-center case, capsule starts from (2.0, −0.1), 0.1 unit length lower than the symmetric axis. The third is termed the near-wall case, in which capsule starts from (2.0, −0.5), 0.5 unit length lower than the symmetric axis, and only 0.2 unit length between the capsule lowest point and the bottom boundary. During simulations, positions and shapes, morphological properties, and center velocities in x and y directions of the capsules are calculated to elucidate the effects of different conditions on the capsule motions.

III. RESULTS AND DISCUSSION

A. Motions of center-line capsules

Evolutions of positions and shapes of three center-line capsules with membrane dilation modulus of 2500 are illustrated in Fig. 5. Positions and shapes of three kinds of center-line capsules with different membrane dilation moduli at time 4.0 are shown in Fig. 6. Both figures show that the front/downstream end of capsule bulges or gets less concave, and the rear/upstream end becomes less convex or more concave, showing more or less similar parachute shapes predicted for capsules [10] and red blood cells [3]. These deformations are undergone by the capsules due to the hydrodynamic stresses on the capsule membrane imposed by the background Poiseuille flow. It can be seen from Fig. 6 that the capsule deforms increasingly with the decreasing membrane dilation modulus. The ratio of the reduced membrane bending stiffness to the reduced membrane dilation modulus is fixed in simulations. Lower membrane dilation modulus together with lower membrane bending stiffness renders the capsule with less resistance to flow force, and leads to larger capsule deformation. The differences in deformations of the elliptic and biconcave capsules are more significant than those of the circular capsules, indicating that, for the center-line cases, the membrane elastic property af-

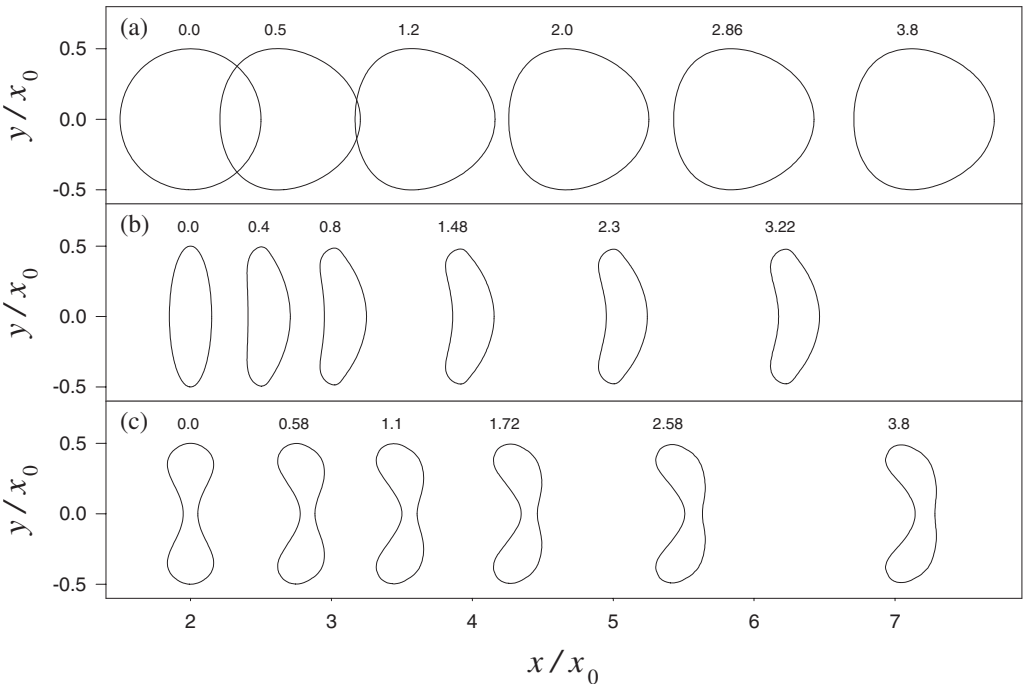

FIG. 5. Evolutions of positions and shapes of the circular (a), elliptic (b), and biconcave (c) center-line capsules with nondimensional membrane elastic dilation modulus of 2500. Number on top of each capsule snapshot indicates corresponding nondimensional time.

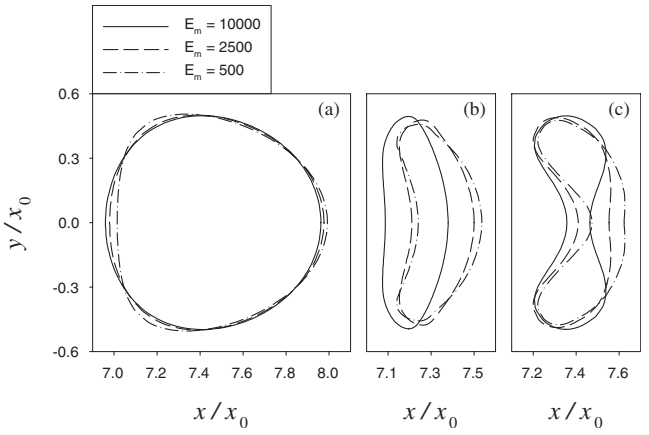

FIG. 6. Positions and shapes of the circular (a), elliptic (b), and biconcave (c) center-line capsules with different membrane dilation moduli at nondimensional time 4.0.

fects more on the elliptic and biconcave capsules than on the circular capsules.

In order to illustrate the capsule deformation quantitatively, evolutions of extension and dispersion of the center-line capsules are shown in Fig. 7. Both extension and dispersion of the circular capsules increase from zero at the beginning, as shown in Fig. 7(a), indicating the deformation from circle. After initial increase, the extension of the circular capsule with membrane dilation modulus of 2500 decreases, and changes abruptly at point "B," after which the extension increases again, similar to the trends in Figs. 3(b) and 4. Before point B, the capsule orientation is 0.5π or -0.5π, i.e., the long axis of the equimomental ellipse is along y direction. After point B, the orientation is 0, i.e., the long axis of the equimomental ellipse changes to along x direction, meaning that the capsule is prolonged in x direction after point B. Similar change occurs to the circular capsule with membrane dilation modulus of 10 000 at point "A," as shown in Fig. 7(a). The extension evolution of the circular capsule with membrane dilation modulus of 500 shows similar trend to the capsule with membrane dilation modulus of 2500 before point B, suggesting that it might be prolonged in x direction at a time beyond the simulation time range. Extension of the elliptic and biconcave center-line capsules decreases with time, suggesting that they become more circular, since their sizes in y direction decrease with time, and their sizes in x direction increase in order to keep their areas fixed. Their dispersion increases with time, similar to the circular capsules, and the long axes of their equimomental ellipses are along y direction in the whole simulation time range.

The hematocrit ratio, $r_h = H_T / H_D$, can be used to demonstrate the rheological properties of capsule flow, where H_T is the tube hematocrit, defined as the volume fraction of the suspended phase, and H_D is the discharge hematocrit, defined as the ratio between the volumetric flow rate of the capsules averaged over a long period of time to the flow rate of the whole suspension. Pozrikidis [3] analyzed the motion of a file of red blood cells in axisymmetric Poiseuille flow through capillaries, and showed that $r_h = U_m / U_c$, where U_m is the mean velocity of undisturbed Poiseuille flow, and U_c is the cell velocity. In the present study, the hematocrit ratio, $r_h = U_m / U_c$, is adopted similarly, where U_m is the mean velocity of undisturbed 2D Poiseuille flow [Eq. (19)], and U_c is the velocity of capsule mass center in x direction. Since the center-line capsule is in the high-velocity region, its flow rate exceeds that of the overall fluid, i.e., r_h is less than unity. It is confirmed that r_h is less than unity for a broad range of conditions [25]. The reduction of r_h from unity is known as the Fåhraeus effect [26]. If the capsule velocity is taken to be equal to the centerline velocity of the 2D Poiseuille flow, the lower bound of r_h can be calculated from $U_c = 1.5 U_m$, that is $r_{h,\min} = 2/3$. As a result, the values of r_h for the center-line capsules are in the range of 2/3—1.0. Because capsule with zero speed is suddenly introduced into the background flow at the beginning of simulation, and the capsule membrane velocities are interpolated from those of fluid grid points, the initial capsule velocity is near to the centerline velocity of undisturbed Poiseuille flow, which means that initial value of

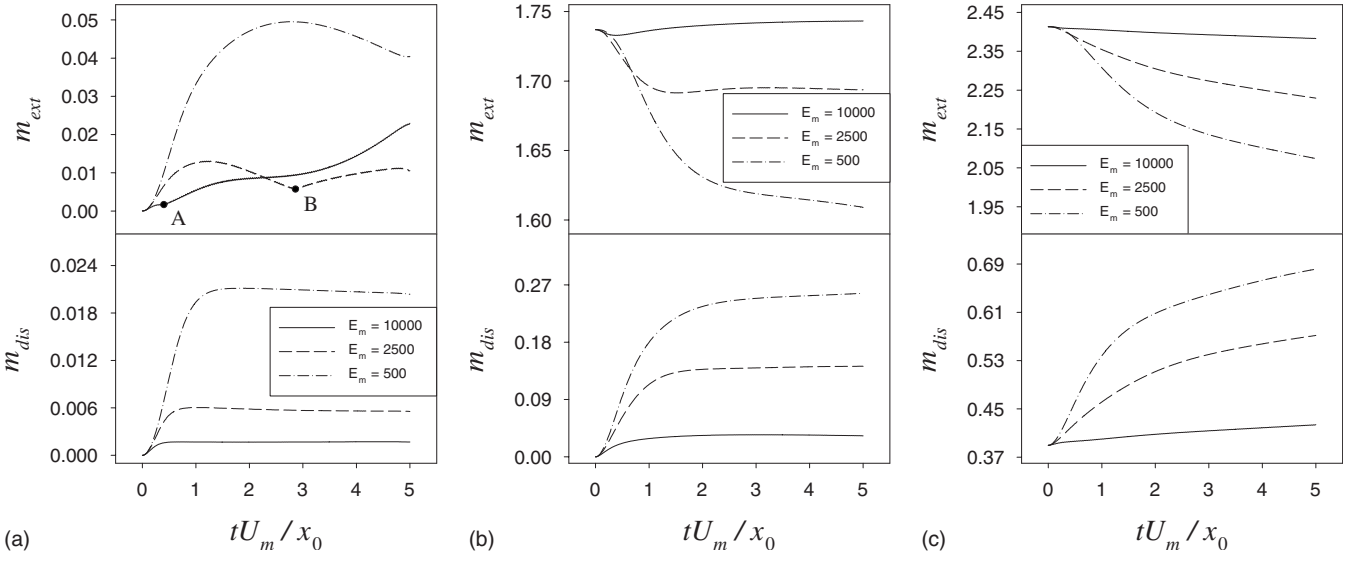

FIG. 7. Temporal variations in the extension and dispersion of the circular (a), elliptic (b), and biconcave (c) center-line capsules.

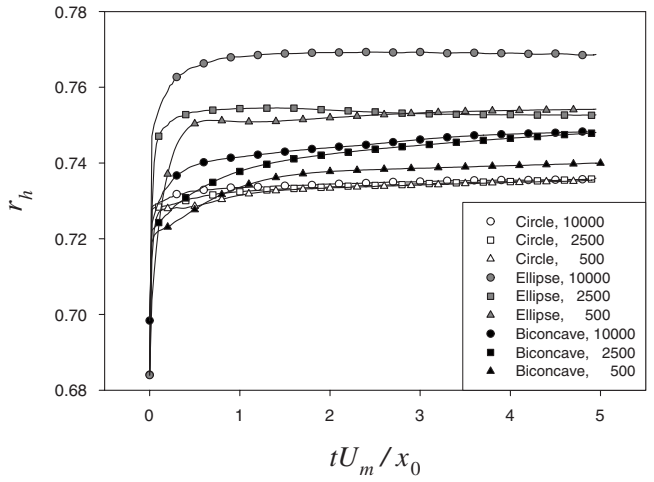

FIG. 8. Evolution of the hematocrit ratios for three kinds of center-line capsules with different nondimensional membrane dilation moduli.

r_h is near to $r_{h,\min}$. The evolutions of the hematocrit ratios for three kinds of center-line capsules with different membrane dilation moduli are shown in Fig. 8. Hematocrit ratios for all cases increase with time after rapid jump from near to the lower bound value at the beginning, and show some asymptotic behaviors except the biconcave capsules with membrane dilation moduli of 10 000 and 2500. Among the three kinds of capsules, the circular capsules obtain the lowest hematocrit ratios, i.e., the highest translational velocities, and the elliptic capsules have the highest hematocrit ratios, i.e., the lowest velocities. Hematocrit ratios for three circular capsules almost coincide, while the differences in membrane mechanical properties lead to significant differences in hematocrit ratios for the elliptic and biconcave capsules, also showing that the membrane dilation modulus affects more on the elliptic and biconcave capsules than on the circular capsules. For the circular and biconcave capsules, the hematocrit ratio increases with the membrane dilation modulus, i.e., the capsule translational velocity decreases with the increasing membrane dilation modulus. If the membrane dilation modulus [Eq. (10)] is fixed, it can be concluded that hematocrit ratio decreases with increasing fluid velocity, showing the same trend as that in [3]. Similar behaviors can be observed for the elliptic capsules before time about 2.88, after which hematocrit ratio for the elliptic capsule with membrane dilation modulus of 2500 is less than that with membrane dilation modulus of 500.

B. Motions of near-center capsules

In general, the configuration of capsule in microscale flow is not necessarily symmetric. The asymmetric motion of capsule is analyzed in the following. Evolutions of positions and shapes of three near-center capsules with membrane dilation modulus of 2500 are illustrated in Fig. 9. In each plot, a solid circle is used to represent a Lagrangian membrane node, and its initial position is on the symmetric axis parallel to the x axis. Positions and shapes of three kinds of near-center capsules with different membrane dilation moduli at time 4.0 are shown in Fig. 10. On each membrane, there is a representative node, whose initial position is the same as in Fig. 9. The deformations of the near-center capsules show similar characteristics to the center-line capsules, i.e., the front end

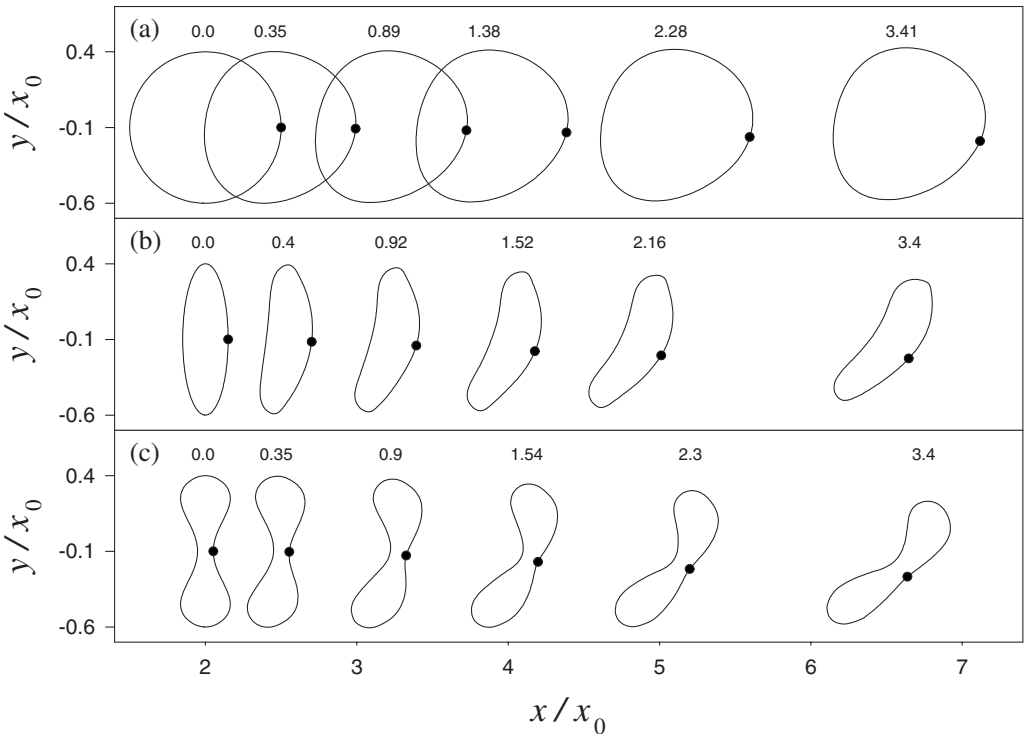

FIG. 9. Evolutions of positions and shapes of the circular (a), elliptic (b), and biconcave (c) near-center capsules with nondimensional membrane dilation modulus of 2500. Number on top of each capsule snapshot indicates corresponding nondimensional time.

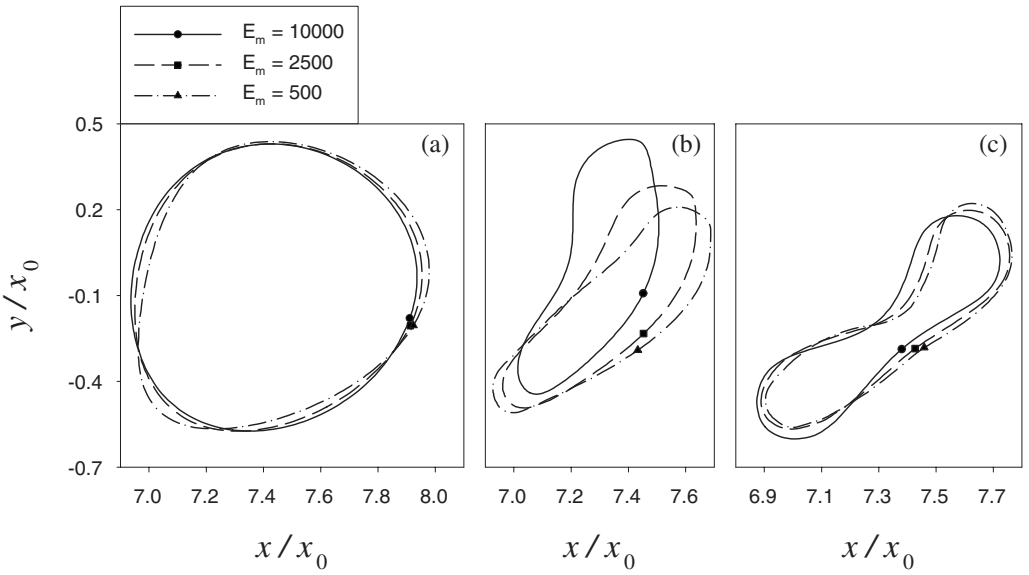

FIG. 10. Positions and shapes of the circular (a), elliptic (b), and biconcave (c) near-center capsules with different membrane dilation moduli at nondimensional time 4.0.

bulges or becomes less concave, and the rear end gets less convex or becomes more concave. All the near-center capsules not only move in positive x direction, but tilt clockwise as well. Since the initial capsule center is 0.1 unit length lower than the centerline, the moving velocity of the upper part is higher than that of the lower part, leading to the clockwise tilt. The motions of the representative nodes in Fig. 9 show that the capsule membrane undergoes clockwise tank-treading motion [8] under the asymmetric conditions. It is also seen from Fig. 10 that, for the near-center cases, the membrane dilation modulus affects more on the elliptic capsules than on the circular and biconcave capsules, different from the center-line cases.

Figure 11 illustrates the distributions of tank-treading velocities, v_{tt}, of the circular and biconcave near-center capsules with membrane dilation modulus of 2500 along capsule arc length, l, at different times. The tank-treading velocity is defined as the tangential component of the difference between the membrane node velocity and the capsule center velocity. Values of the tank-treading velocities are mainly negative, since anticlockwise motion is defined as positive here. The tank-treading velocities of both capsules change greatly along arc length in early period of simulation, indicating the existence of in-plane stretching or compression deformation in membrane, and the variations decrease with time. The variation in the tank-treading velocity of the biconcave capsule is much larger, about five times that of the circular capsule at the end of the time range. Tank-treading velocity of the elliptic near-center capsule shows similar characteristics to the biconcave capsule, and its variation is between those of the other two kinds of capsules. The elliptic and biconcave capsules try to keep their curvature akin to the initial value, preventing their membrane nodes from moving in the tank-treading motion "freely," and leading to larger tank-treading velocity variations than the circular capsule. The mean tank-treading velocities at time 5.0 are shown in

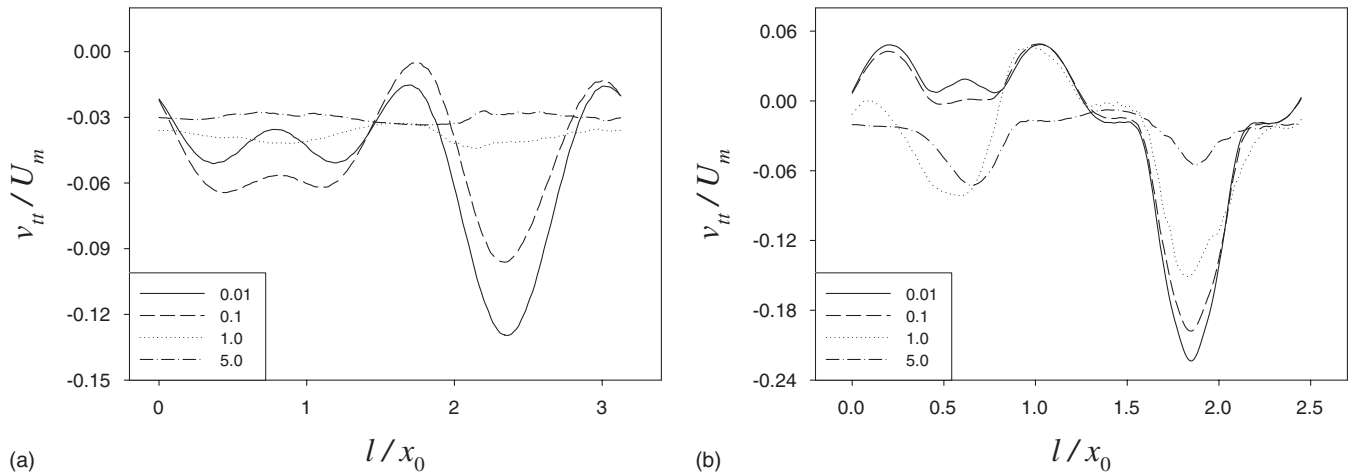

FIG. 11. Distributions of membrane tank-treading velocities of the circular (a) and biconcave (b) near-center capsules with nondimensional membrane dilation modulus of 2500 at different nondimensional time.

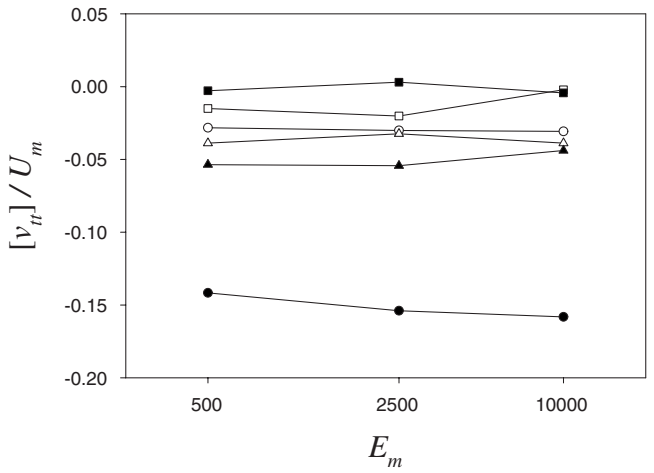

FIG. 12. Mean tank-treading velocities of the near-center and near-wall capsules at nondimensional time 5.0 with respect to membrane dilation modulus. Circular, rectangular, and triangular symbols correspond to the circular, elliptic, and biconcave capsules, and hollow and solid symbols correspond to the near-center and near-wall capsules, respectively.

Fig. 12, in which hollow circle, rectangle, and triangle correspond to the circular, elliptic, and biconcave near-center capsules. The differences of the mean tank-treading velocities among the three kinds of near-center capsules are not significant in spite of significantly different levels of their tank-treading velocity variations, and the effects of membrane dilation modulus are not significant either. The absolute mean tank-treading velocities are less than 0.05, while the capsule moving velocities are 1.3–1.4, calculated from Fig. 14(a), that is, the tank-treading velocities are about 2 orders lower than the capsule velocities. Similar results were predicted for the nonaxisymmetric red blood cells in cylindrical capillaries [27].

Evolutions of extension, dispersion, and orientation of the near-center capsules are illustrated in Fig. 13. Extension and dispersion of the circular near-center capsules increase from zero initially, and then experience no great change after maxima, or reach some plateaus. Interestingly, oscillations occur in orientation of the circular near-center capsules with membrane dilation moduli of 10 000 and 2500. The capsule behaviors in the present discussion are some combination of the center-line motion and the motion in shear flow. It is well known that, in shear flow, the liquid capsule undergoes oscillations in orientation when the viscosity ratio of the internal to the external fluids is large [28], but the viscosity ratio is 1.0 here. As to the elliptic and biconcave capsules, the extension goes down at the beginning, and then increases after having reached the minima, and the dispersion increases at first, then decreases after having reached the maxima. These trends are totally different from those of the center-line capsules. Orientation of all the elliptic and biconcave capsules undergoes monotonic decrease from 0.5π. Noting the larger differences of orientation among the elliptic capsules than the circular and biconcave capsules, it is concluded again that the membrane dilation modulus affects more on the elliptic capsules than on the circular and biconcave capsules in the near-center cases.

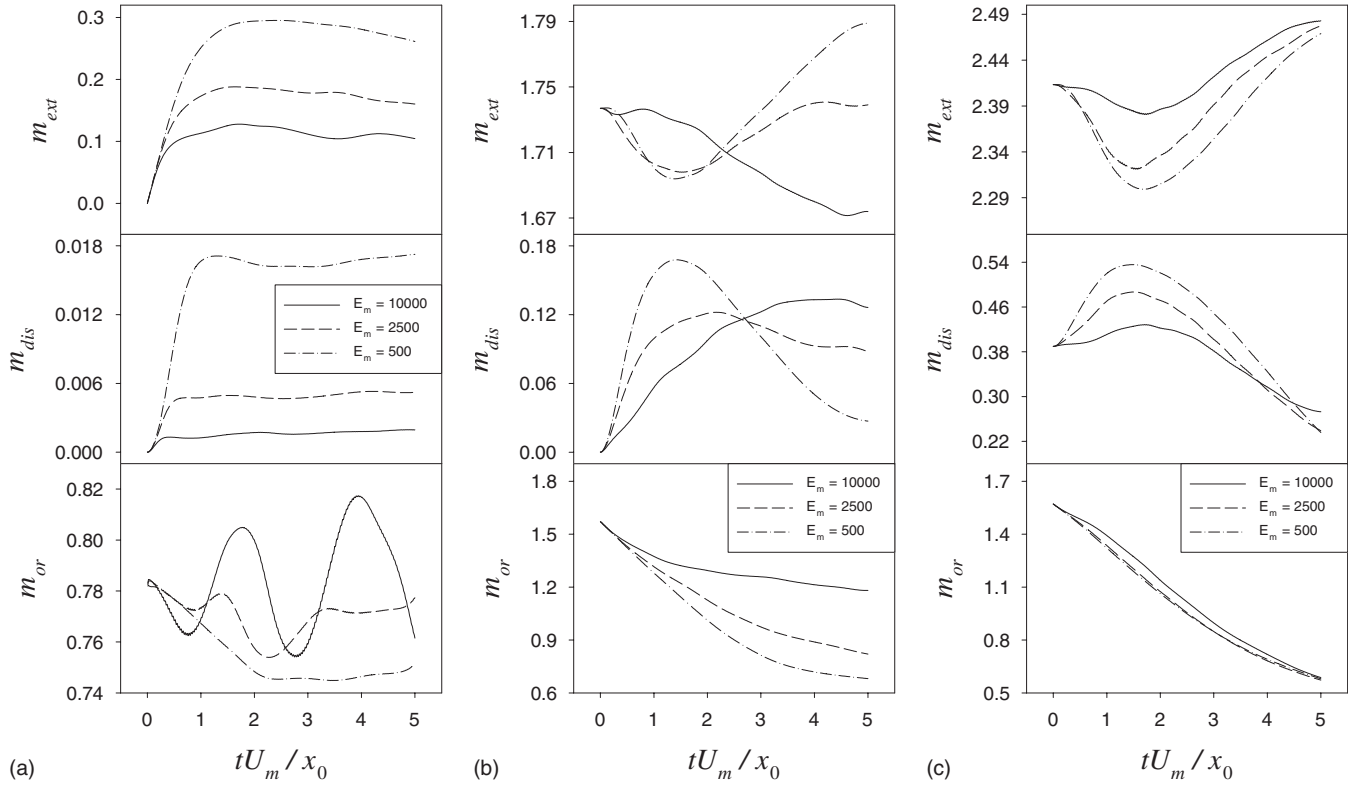

FIG. 13. Temporal variations in extension, dispersion, and orientation of the circular (a), elliptic (b), and biconcave (c) near-center capsules.

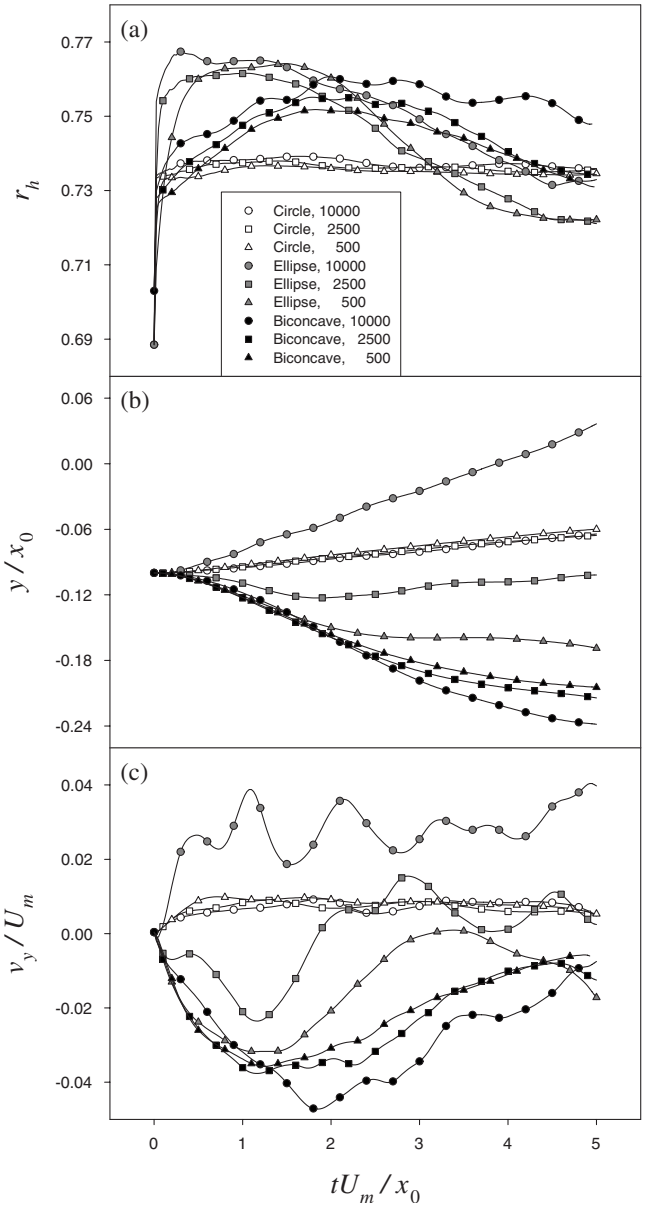

FIG. 14. Evolution of the hematocrit ratios (a), y coordinates of capsule centers (b), and capsule velocities in y direction (c) for three kinds of near-center capsules with different nondimensional membrane dilation moduli.

For the near-center cases, the hematocrit ratio is also used to illustrate the effects of the capsule initial shape and membrane dilation modulus on the capsule motion, as shown in Fig. 14(a). Before time about 2.0, the circular capsules have the lowest hematocrit ratios, i.e., the highest velocities in x direction, and the elliptic capsules have the highest hematocrit ratios, i.e., the lowest velocities. In the whole time range, the hematocrit ratios of the circular near-center capsules almost remain the same as those of the circular center-line capsules, showing that small deviation of the initial position from the centerline has little effect on the motions of the circular capsules in line of the moving velocity in flow direction. Hematocrit ratios of the other two kinds of near-center capsules decrease after reaching maxima. At the end of the simulations, the elliptic and biconcave capsules have the lowest and highest hematocrit ratios, corresponding to the highest and lowest translational velocities, respectively. The hematocrit ratio results of the circular and biconcave near-center capsules demonstrate that higher hematocrit ratio correspond to higher membrane dilation modulus, similar to the center-line capsules in the present study and to the red cells in [3], while the hematocrit ratios of the elliptic near-center capsules with membrane dilation moduli of 2500 and 500 show inverse trend in some time range.

One important feature of the off-center capsules (near-center and near-wall capsules) in flow is the lateral migration away from the wall, because of which a capsule-free layer near the capillary wall tends to develop. The lateral migration is initiated by several factors, such as the presence of a wall, the nonlinearity of the shear flow, and the nonlinear character of the fluid. It is known that, in the limit of low Reynolds number, a capsule does not exhibit a lateral migration with respect to the flow direction in an unbounded linear shear flow. In the presence of a wall, a capsule in linear shear flow is found to migrate away from the wall because the translational symmetry perpendicular to the flow direction is broken [29]. Nonlinear character of the Poiseuille flow together with the capsule deformation causes a cross-streamline migration of the capsule toward the flow center even if the Poiseuille flow is unbounded [12]. It is also shown that the rigid sphere can migrate laterally due to the nonlinear contribution of term $\nabla \cdot \rho \mathbf{uu}$ in the Navier-Stokes equations [30]. All the three factors, namely, the presence of wall, the nonlinearity of the Poiseuille flow, and the nonlinear character of the fluid, are included in the present simulations. In order to illustrate the lateral motions of the capsules, evolutions of the capsule center positions and the capsule center velocities in y direction are shown in Figs. 14(b) and 14(c), where the capsule center velocity in y direction is termed the lift velocity. Upward movement and positive lift velocities of the circular near-center capsules indicate the existence of lift effect of fluid flow causing the capsule to move away from the wall. All the three biconcave capsules move downward in the whole time range. Elliptic near-center capsules with different membrane dilation moduli perform differently, namely, the elliptic capsule with membrane dilation modulus of 10 000 moves upward, the capsule with modulus of 2500 moves downward at first and then upward after time about 2.0, and the capsule with modulus of 500 moves downward, showing great effects of membrane mechanical property on the capsule behaviors. The nonuniform distribution of the capsule moving velocities interpolated from the fluid velocities leads to not only clockwise tilt, but downward movements of the elliptic and biconcave near-center capsules as well. Figure 14(c) shows that the lift velocities of the biconcave capsules and low-modulus elliptic capsules become less negative after having reached the minima, suggesting that the lift effect might also exist in these cases. The absolute lift velocities for the near-center capsules are about 0.01–0.04, about 2 orders lower than the capsule velocities in flow direction. Sukumaran and Seifert [31] also found that the lift velocities of 3D near-wall vesicles are much less than translational velocities.

It is found from Figs. 14(a) and 14(b) that, the elliptic near-center capsule with membrane dilation modulus of

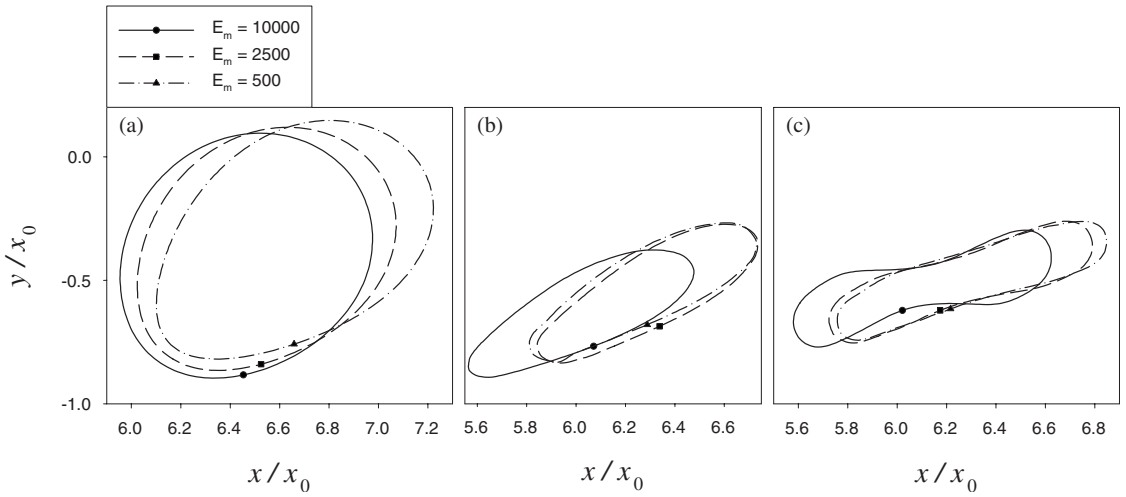

FIG. 15. Positions and shapes of the circular (a), elliptic (b), and biconcave (c) near-wall capsules with different membrane dilation moduli at nondimensional time 4.0.

10 000 is the closest to the centerline at the end of simulation, but it does not have the highest moving velocity. The translational velocities of the biconcave and low-modulus elliptic near-center capsules are larger than or equal to those of the circular capsules despite the former are farther from the centerline than the latter. The clockwise tilt of the biconcave and low-modulus elliptic capsules reduces their effective sizes perpendicular to the direction of the background flow. The capsule tilt and the membrane tank-treading motion might be the main reasons for the reduction of flow resistance and the increase of moving velocities.

C. Motions of near-wall capsules

Positions and shapes of three kinds of near-wall capsules with different membrane dilation moduli at time 4.0 are shown in Fig. 15, in which there is a representative node on each curve, and its initial position is on the symmetric axis parallel to the x axis. Transient deformations of near-wall capsules are similar to those of the near-center capsules, except that the near-wall capsules are more tilted than the near-center capsules. Positions of the representative nodes suggest the existence of the membrane tank-treading motion. The mean tank-treading velocities of the near-wall capsules at time 5.0 are also shown in Fig. 12, where solid circular, rectangular, and triangular symbols represent the circular, elliptic, and biconcave near-wall capsules, respectively. It is shown that the absolute mean tank-treading velocities of the circular capsules increase greatly compared with the results of the near-center capsules, while mean tank-treading velocities of the elliptic and biconcave capsules do not change much. Uniform resting curvatures along the membrane of the circular capsules place no restriction on the movements of membrane nodes to adapt the capsules to higher flow shear rate at farther distance from the centerline by faster tank-treading motion, while the elliptic and biconcave capsules restrict the free tank-treading motion of the membrane nodes in order to maintain the membrane curvature akin to the initial value. It was predicted by Hsu and Secomb [27] that the membrane tank-treading velocity is much smaller than the cell velocity. In the present study, the absolute tank-treading velocities of the near-wall capsules are 0.003–0.15, and the cell translational velocities range from 0.9 to 1.3, calculated from Fig. 17(a), i.e., the tank-treading velocity is about 1–2 orders lower than the capsule velocity.

Evolutions of extension, dispersion, and orientation of the near-wall capsules are illustrated in Fig. 16. Extension and dispersion of the circular near-wall capsules go up from zero at the beginning, and then decrease with time from maxima. Those of the elliptic capsules show some oscillations in the present time range, quite different from other cases. Extension of the biconcave near-wall capsules increases at the beginning and then decreases afterward, while their dispersion decreases with time, indicating that the capsules are getting more elliptic. Orientation of all the near-wall capsules decreases rapidly at the beginning, with orientation of the circular capsules decreasing from 0.25π, and that of the elliptic and biconcave capsules decreasing from 0.5π. After that, the circular capsules reach quasistationary tilt orientation, which is similar to the behaviors of the vesicles in unbound Poiseuille Stokes flow [12], and different from the oscillating characteristics of the circular near-center capsules with high membrane dilation moduli. The same behavior is observed in the elliptic near-wall capsules. Quasistationary tilt orientation of the circular capsules ranges from 0.18π to 0.23π, and that of the elliptic capsules from 0.13π to 0.18π. The biconcave near-wall capsules experience steady decrease in orientation with time after initial rapid tilting, as shown in the third plot of Fig. 16(c). This behavior has not been reported in open literature. Probably the biconcave near-wall capsules might reach quasistationary tilt orientation at later time if the simulation time range is extended. Noting the scale ranges of the orientation axes in Fig. 16, it is seen that the effects of membrane dilation modulus on the capsule orientation are small.

Temporal evolutions of hematocrit ratio, and positions and velocities in y direction of the near-wall capsule are shown in Fig. 17. In Fig. 17(a), the hematocrit ratios of all the capsules increase at first and then decrease with time

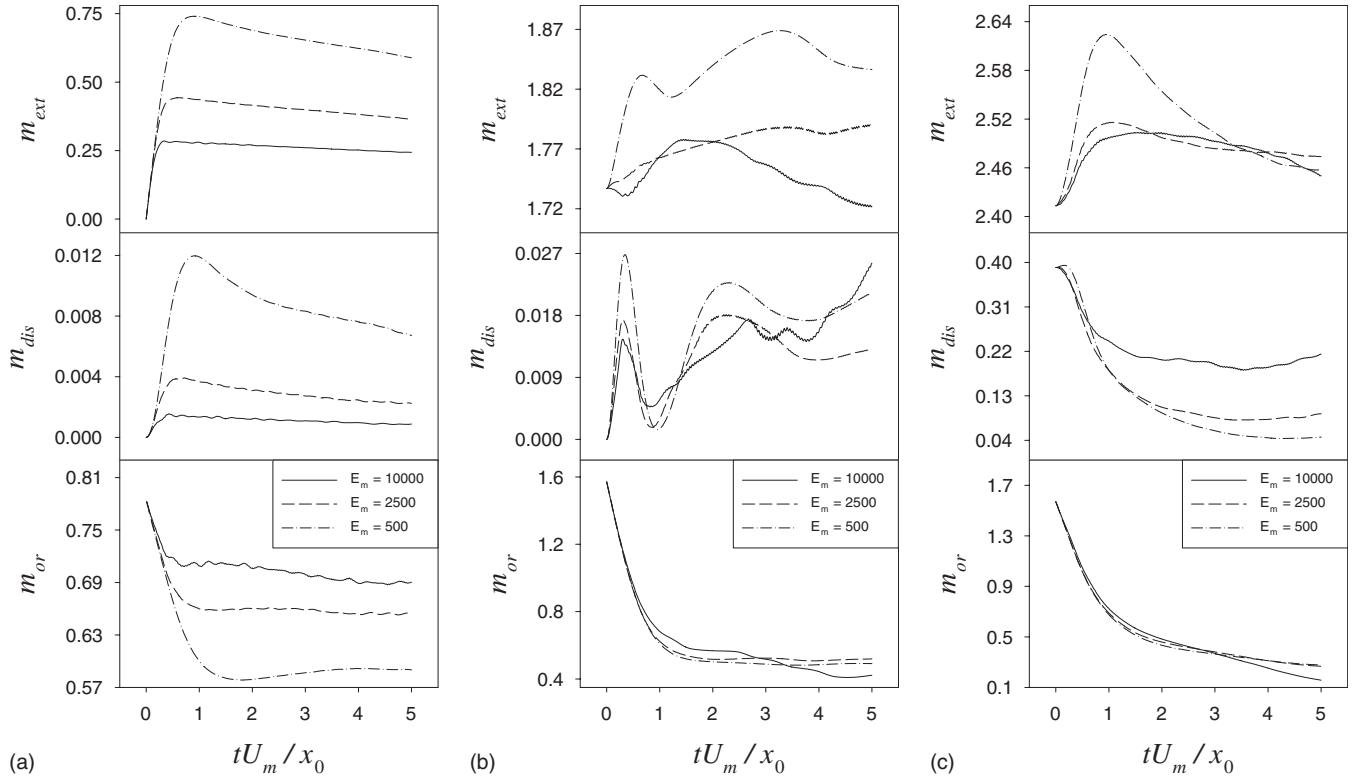

FIG. 16. Temporal variations in the extension, dispersion, and orientation of the circular (a), elliptic (b), and biconcave (c) near-wall capsules.

after reaching the maxima, except the elliptic capsule with membrane dilation modulus of 10000, whose hematocrit ratio shows some oscillations. Higher hematocrit ratio corresponds to higher membrane dilation modulus for the circular and biconcave near-wall capsules, while results of the elliptic near-wall capsules with membrane dilation moduli of 2500 and 500 show inverse characteristics in some time range, which is similar to the center-line and near-center cases. The near-wall capsules have higher hematocrit ratios or lower translational velocities than the center-line and near-center capsules, since they are the farthest from the centerline. As shown in Fig. 17(b), the center positions in y direction of the circular near-wall capsules increase in the whole time range, and their lift velocities are positive, as shown in Fig. 17(c), indicating that the flow has lift effect on the circular near-wall capsules. The elliptic and biconcave near-wall capsules move downward in the flow at first, and move upward afterward, even the elliptic capsule with membrane dilation modulus of 10000 also move upward after time 4.5, also showing the existence of lift effect of the flow. The nonuniform distribution of the capsule moving velocities, which are interpolated from the fluid velocities, is the main reason accounting for the initial downward movement of the elliptic and biconcave capsules, and its effect trail off with time. After certain time, the lift effect of the flow prevails, resulting in the upward movement of capsules. The capsules move upward almost linearly with time, similar to the behaviors of vesicles in unbound Poiseuille Stokes flow [12]. Combining Fig. 17(a) with Fig. 17(b), it is understood that the capsule velocities in x direction in most cases increase gradually after having reached the minima, mainly because the capsules move closer to the centerline, experiencing the increasing background flow velocity. Generally, the capsule with higher membrane dilation modulus has lower lift velocity, as show in Fig. 17(c). As a result, the lift velocity depends on not only the distance from the capsule and the wall [31], but capsule deformability as well. The absolute lift velocities of the near-wall capsules range 0.01–0.06, again about 2 orders lower than the capsule velocities in x direction. In unbound Poiseuille Stokes flow [12], the vesicle migration velocity is found to increase with the local capillary number, which is proportional to the distance from the vesicle to the centerline, and reaches a plateau above a certain value of the capillary number. Lift velocities of the circular near-wall capsules in Fig. 17(c) decrease as they approach the centerline, showing similar trends to the vesicles in [12]. Migration velocities of the elliptic near-wall capsules do not show this kind of trend. Lift velocities of the biconcave near-wall capsules increase in large time range, different from the circular cases, but they decrease after time about 4.0. Further research work is needed to study the behaviors of the capsules in extended time range.

D. Results of a preliminary long-term simulation

A preliminary study is carried out for long-term simulation of a circular capsule, in which the Reynolds number is 0.01, the density and viscosity ratios of inner fluid to outer fluid are 1.098 and 1.0, respectively, which are the same as the previous short-term simulations. The nondimensional membrane elastic modulus is 1.0×10^4. The initial position of the capsule is (2.5, −0.5), where 2.5 is chosen as the initial

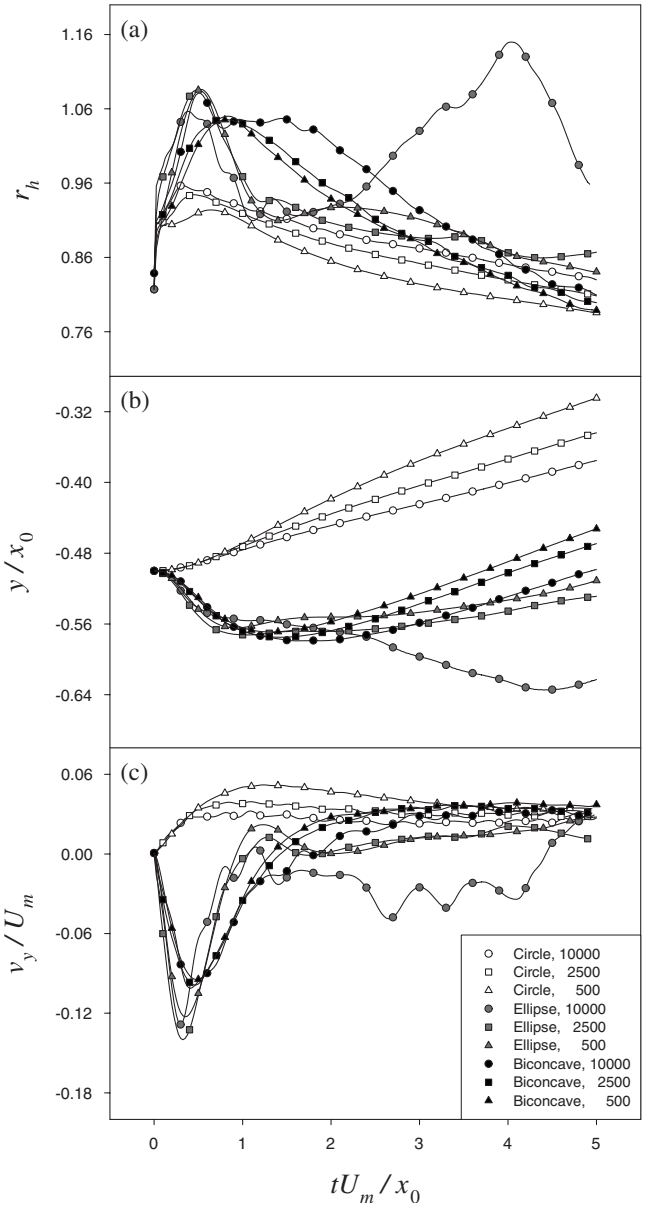

FIG. 17. Evolution of the hematocrit ratios (a), y coordinates of capsule centers (b), and capsule velocities in y direction (c) for three kinds of near-wall capsules with different nondimensional membrane dilation moduli.

x coordinate of capsule center to minimize the effect of tube ends. In the previous short-term simulations, however, 2.0 is chosen as the initial x coordinate according to results shown in Fig. 4. The present input data are similar to those for one of the previous near-wall cases. The nondimensional length of computational domain is 6, shorter than those in the cases of short-term simulations. After the capsule is released, it moves rightward with background flow. The capsule position is checked each every 10^3 time steps. If the capsule center is located less than 2.5 to the right end of the tube, the computational domain will be moved in positive x direction over a distance, such that the capsule center will be near to but not less than 2.5 to the new left end of the tube. The computed values, such as density and velocity, will also be transferred accordingly. After the computational domain is modified in this way, computation can be carried out continuously.

Evolution of the position and shape of the capsule is shown in Fig. 18. Number on top of each capsule snapshot indicates the corresponding time. In the initial period just after release, the capsule is subjected to high force and undergoes large deformation, which is found at the left end in the curve of the extension-time relation shown in Fig. 19(a). After that, the elastic property of the capsule membrane causes the capsule to restore its initial shape, namely, the capsule extension decreases with time. Figure 19(b) shows the variation in the capsule orientation with time. In most time period from time 0 to about 35, the capsule orientation does not change much, staying around $0.22\pi \sim 0.24\pi$ that is similar to the simulation of circular near-wall capsule shown in Fig. 16(a). As the capsule approaches the tube center line, its orientation goes down rapidly. When the capsule center reaches the tube center line, the orientation is zero. Figure 18 illustrates clearly the tank-treading motion of capsule membrane by the motion of a representative point. It is also observed that the tank-treading motion fades out as the capsule moves toward the centerline. Figure 19(c) shows the temporal variation in the angle of a line with respect to x axis, which starts from the capsule center and ends at the representative point. This angle is represented by a_{tt}. When the capsule is near to the wall, it undergoes higher shear rate of flow. The shear rate it undergoes decreases when it approaches the centerline. From time 0 to 10, the representative point turns about half circle. From time 32 to 40 when the capsule is located near to the centerline, the tank-treading motion is much less than that in the initial period. The simulation result shows an interesting phenomenon. When capsule center reaches the tube center line at time about 39.44, which is obtained from the y coordinate-time relation, shown in Fig. 19(e), the capsule has symmetric shape, which is seen from the capsule snapshot at time 40 in Fig. 18. This characteristic is similar to the results of Kaoui *et al.* [12].

It is observed from Fig. 18 that the capsule moves from left to right ends with the background flow, and the moving speed increases with time. The capsule is subjected to lower background flow velocity when it is located near to the wall, while the background flow velocity increases when the capsule approaches the centerline. The variation of capsule center velocity in x direction with time is shown quantitatively in Fig. 19(d). Meanwhile, the capsule moves upward, which can also be observed from the curve of y coordinate-time relation as shown in Fig. 19(e), and the result of capsule center moving velocity in y direction as shown in Fig. 19(f). This clearly shows the lift effect of the flow. Figures 19(e) and 19(f) also demonstrate that the capsule moves quite fast at first. After that, it moves with lower speed and almost linearly with time. As the capsule moves closely to the centerline, its lateral moving velocity increases again, which is different from the results of Kaoui *et al.* [12]. It is not clear whether the lateral velocity jump is a physical phenomenon or results from numerical algorithm.

IV. CONCLUSION

The initial motion of 2D capsule in microchannel flow is studied numerically based on a numerical simulation

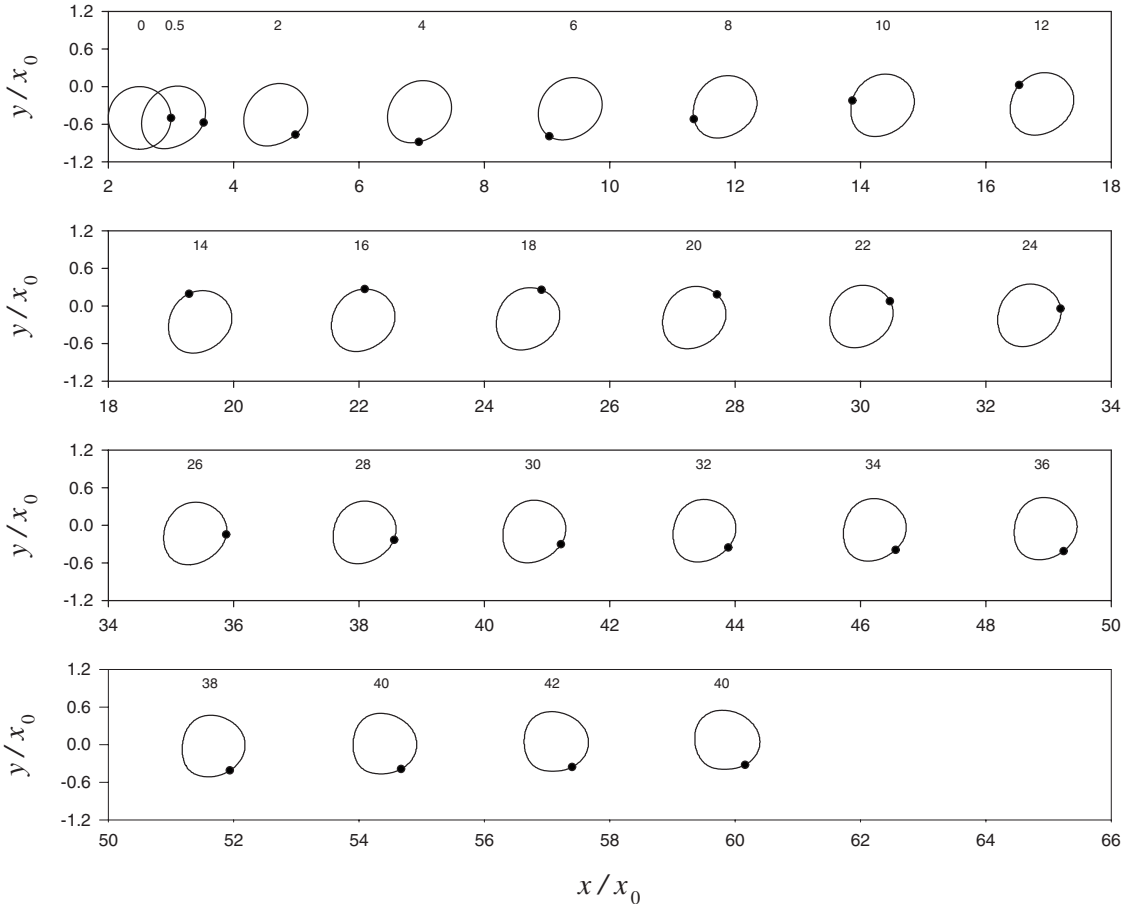

FIG. 18. Evolution of position and shape of the circular near-wall capsule with nondimensional membrane dilation modulus of 1.0×10^4. Number on top of each capsule snapshot indicates the corresponding nondimensional time.

method, which is a combination of the finite volume method for solving fluid problem on fixed Eulerian grid with the front tracking technique for capturing and tracking the capsule membrane discretized by Lagrangian nodes.

For all the three kinds of center-line capsules, namely, the circular, elliptic, and biconcave capsules, the front/downstream end of the capsule bulges or gets less concave, and the rear/upstream end becomes less convex or more concave, showing more or less the parachute shapes. During the movement of the circular center-line capsules, their deformation results in the change in the long axes of the equimomental ellipses from along the transverse direction to along the fluid flow direction.

The off-center capsules, namely, the near-center and near-wall capsules, experience tilting and membrane tank-treading, and migrate laterally while moving along the fluid flow. Uniform resting curvature along the membrane of the circular capsules place no restriction on the movements of membrane nodes to adapt to shear flow by tank-treading motion, while the elliptic and biconcave capsules try to keep the membrane curvature akin to the initial value, preventing the membrane nodes from moving in tank-treading motion "freely." In the present simulations, the tank-treading velocities are about 1–2 orders lower than the capsule moving velocities. Most off-center capsules are tilted asymptotically with time, while the circular near-center capsules with membrane dilation moduli of 10 000 and 2500 undergo oscillations in orientation. After initial rapid decrease in orientation, the circular and elliptic near-wall capsules reach quasistationary tilt orientation, similar to the behaviors of vesicles in unbound Poiseuille Stokes flow [12]. The biconcave near-wall capsules experience steady decrease in orientation after initial rapid tilting, instead of keeping a quasistationary tilt orientation. This behavior has not been reported in literature. The nonuniform distribution of the capsule moving velocities interpolated from the fluid velocities is the main reason accounting for not only the clockwise tilting, but the movement of elliptic and biconcave capsules away from the centerline at the beginning as well. The lift velocities of the elliptic and biconcave near-center capsules get less negative after having reached the minima in spite of their downward movement. The elliptic and biconcave near-wall capsules migrate toward the centerline after certain time. These results together with the migration of the circular off-center capsules away from the wall indicate the existence of lift effect of the fluid flow. Lift velocities of the circular near-wall capsules decrease as they approach the centerline, showing similar trends to the vesicles in [12]. If the time range of simulations is extended, the migration velocities of the elliptic and biconcave near-wall capsules might show the same trends. Lift velocities are about 2 orders lower than capsule velocities. In general, the capsule with higher membrane dilation modulus has lower

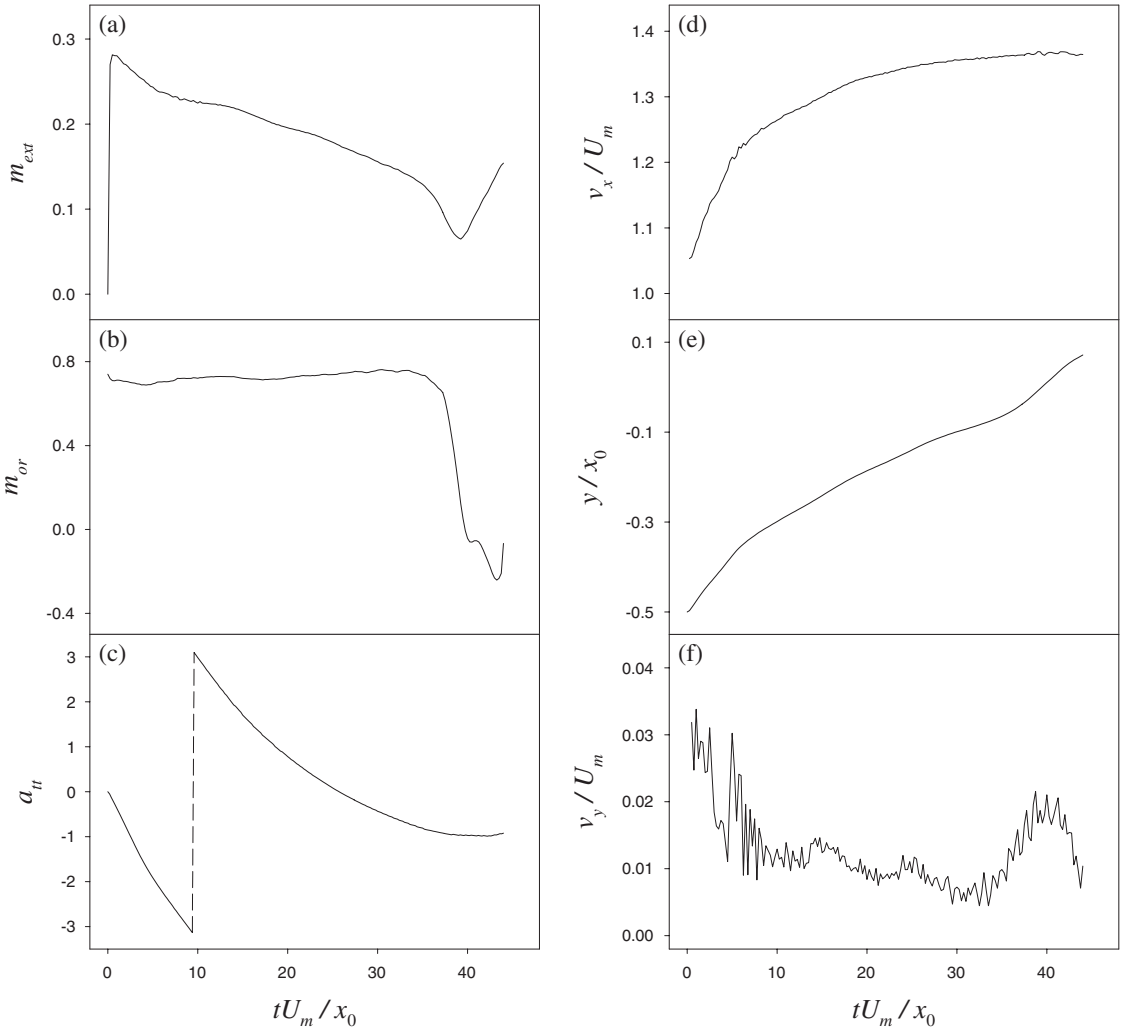

FIG. 19. Temporal evolutions of extension (a), capsule orientation (b), capsule velocity in x direction (d), y coordinate of capsule center (e), capsule velocity in y direction (f), and angle of the line with respect to x axis which starts from the capsule center and ends at the representative point (c).

lift velocity, showing the effect of capsule deformability on the capsule behavior.

It is concluded that, the hematocrit ratio of the circular and biconcave capsules, no matter the center-line or off-center capsules, increases with membrane dilation modulus, that is, the capsule moving velocity decreases with increasing membrane dilation modulus, showing similar trends to red cells in [3], while the elliptic capsules with membrane dilation moduli of 2500 and 500 show inverse trend in some time range.

A preliminary study is conducted for long-term simulation of a circular capsule. Figures 18 and 19(c) clearly show the tank-treading motion of capsule membrane, which fades out as the capsule moves toward the centerline. The capsule moves to the centerline when it moves from left to right ends with the background flow, which indicates the existence of the lift effect of the flow. When the capsule center reaches the tube center line, the capsule forms a symmetric shape. A detailed study will be conducted to elucidate the characteristics of long-term lateral migration of the off-center capsules in future work.

ACKNOWLEDGMENTS

The authors gratefully acknowledge the financial support from the Ministry of Education of Singapore through Academic Research Fund (AcRF) Tier 1 under Project No. M52056029 (RGM 7/07).

APPENDIX: MORPHOLOGICL ANALYSIS OF 2D SHAPE

Morphological characteristics of 2D area S enclosed by a closed curve are analyzed as follows. n nodes are employed to discretize the closed curve, and n straight segments connecting the neighboring nodes to approximate the curve. Let the coordinate of the ith node be (x_i, y_i), and let $(x_{n+1}, y_{n+1}) = (x_1, y_1)$. The zero-, first-, and second-order moments of the shape are calculated as

$$m_{00} = \int \int_S dxdy = \sum_{i=1}^{n} A_i = \text{area},$$

$$m_{10} = \int\int_S x dx dy = \sum_{i=1}^{n} A_i \frac{1}{3}(x_i + x_{i+1}),$$

$$m_{01} = \int\int_S y dx dy = \sum_{i=1}^{n} A_i \frac{1}{3}(y_i + y_{i+1}),$$

$$m_{20} = \int\int_S x^2 dx dy = \sum_{i=1}^{n} A_i \frac{1}{6}(x_i^2 + x_i x_{i+1} + x_{i+1}^2),$$

$$m_{11} = \int\int_S xy dx dy = \sum_{i=1}^{n} A_i \frac{1}{12}(2x_i y_i + 2x_{i+1} y_{i+1} + x_i y_{i+1} + x_{i+1} y_i),$$

$$m_{02} = \int\int_S y^2 dx dy = \sum_{i=1}^{n} A_i \frac{1}{6}(y_i^2 + y_i y_{i+1} + y_{i+1}^2), \quad \text{(A1)}$$

where $A_i = 0.5(x_i y_{i+1} - x_{i+1} y_i)$. From the zero-and first-order moments, the centroid of the 2D shape is calculated by the following equations:

$$x_c = m_{10}/m_{00}, \quad y_c = m_{01}/m_{00}. \quad \text{(A2)}$$

Three second-order central moments are calculated as

$$\mu_{20} = m_{20} - (m_{10}^2/m_{00}), \quad \mu_{02} = m_{02} - (m_{01}^2/m_{00}),$$

$$\mu_{11} = m_{11} - (m_{10} m_{01}/m_{00}). \quad \text{(A3)}$$

Based on the above variables, three normalized central moments, which are invariant to change in size of the 2D shape, are given as follows:

$$\eta_{20} = \mu_{20}/m_{00}^2, \quad \eta_{11} = \mu_{11}/m_{00}^2, \quad \eta_{02} = \mu_{02}/m_{00}^2. \quad \text{(A4)}$$

Two second-order measures of shape that are invariant to rotation are expressed as

$$\phi_1 = \eta_{20} + \eta_{02}, \quad \phi_2 = (\eta_{20} - \eta_{02})^2 + 4\eta_{11}^2. \quad \text{(A5)}$$

The two rotational invariants can be calculated

$$\lambda_1 = 2\pi(\phi_1 + \sqrt{\phi_2}), \quad \lambda_1 = 2\pi(\phi_1 - \sqrt{\phi_2}). \quad \text{(A6)}$$

The morphological measures, extension, dispersion, and orientation of 2D shape can be determined by

$$m_{\text{ext}} = \log_2(\lambda_1), \quad m_{\text{dis}} = \log_2(\sqrt{\lambda_1 \lambda_2}),$$

$$m_{\text{or}} = 0.5 \arctan[2\eta_{11}/(\eta_{20} - \eta_{02})]. \quad \text{(A7)}$$

[1] R. Skalak and P. I. Branemark, Science **164**, 717 (1969).
[2] T. W. Secomb and R. Hsu, Biophys. J. **71**, 1095 (1996).
[3] C. Pozrikidis, Phys. Fluids **17**, 031503 (2005).
[4] B. Lorz, R. Simson, J. Nardi, and E. Sackmann, Europhys. Lett. **51**, 468 (2000).
[5] R. Skalak, N. Ozkaya, and T. C. Skalak, Annu. Rev. Fluid Mech. **21**, 167 (1989).
[6] T. W. Secomb, Microvasc. Res. **34**, 46 (1987).
[7] D. Halpern and T. W. Secomb, J. Fluid Mech. **203**, 381 (1989).
[8] T. W. Secomb and R. Skalak, Microvasc. Res. **24**, 194 (1982).
[9] A. Leyrat-Maurin and D. Barthes-Biesel, J. Fluid Mech. **279**, 135 (1994).
[10] C. Queguiner and D. Barthes-Biesel, J. Fluid Mech. **348**, 349 (1997).
[11] Y. Lefebvre and D. Barthes-Biesel, J. Fluid Mech. **589**, 157 (2007).
[12] B. Kaoui, G. H. Ristow, I. Cantat, C. Misbah, and W. Zimmermann, Phys. Rev. E **77**, 021903 (2008).
[13] B. J. Daly, J. Comput. Phys. **4**, 97 (1969).
[14] C. W. Hirt and B. D. Nichols, J. Comput. Phys. **39**, 201 (1981).
[15] N. Ashgriz and J. Y. Poo, J. Comput. Phys. **93**, 449 (1991).
[16] J. Glimm, J. Grove, B. Lindquist, O. A. McBryan, and G. Tryggvason, SIAM (Soc. Ind. Appl. Math.) J. Sci. Stat. Comput. **9**, 61 (1988).
[17] A. L. Fogelson and C. S. Peskin, J. Comput. Phys. **79**, 50 (1988).
[18] S. O. Unverdi and G. Tryggvason, J. Comput. Phys. **100**, 25 (1992).
[19] J. Hua and J. Lou, J. Comput. Phys. **222**, 769 (2007).
[20] C. Pozrikidis, *Modeling and Simulation of Capsules and Biological Cells*, edited by C. Pozrikidis (Chapman & Hall/CRC, Boca Raton, 2003).
[21] C. S. Peskin, J. Comput. Phys. **25**, 220 (1977).
[22] E. Evans and Y.-C. Fung, Microvasc. Res. **4**, 335 (1972).
[23] C. Migliorini, Y. H. Qian, H. D. Chen, E. B. Brown, R. K. Jain, and L. L. Munn, Biophys. J. **83**, 1834 (2002).
[24] G. A. Dunn and A. F. Brown, J. Cell Sci. **83**, 313 (1986).
[25] A. R. Pries, D. Neuhaus, and P. Gaehtgens, Am. J. Physiol. Heart Circ. Physiol. **263**, H1770 (1992).
[26] R. Fåhraeus, Physiol. Rev. **9**, 241 (1929).
[27] R. Hsu and T. W. Secomb, J. Biomech. Eng. **111**, 147 (1989).
[28] C. Misbah, Phys. Rev. Lett. **96**, 028104 (2006).
[29] I. Cantat and C. Misbah, Phys. Rev. Lett. **83**, 880 (1999).
[30] J. Feng, H. H. Hu, and D. D. Joseph, J. Fluid Mech. **277**, 271 (1994).
[31] S. Sukumaran and U. Seifert, Phys. Rev. E **64**, 011916 (2001).